Numerical investigation on the uniaxial compressive behaviours of an epoxy resin and a nanocomposite[i]

Dayou Ma[a*], Marco Giglio[a], Andrea Manes[a]

[a] Politecnico di Milano, Department of Mechanical Engineering, via la Masa 1, 20156 Milan, Italy. dayou.ma@polimi.it, marco.giglio@polimi.it, andrea.manes@polimi.it.

Abstract

The current work aims at exploring the relationship between complex failure behaviours and the presence of defects for RTM6 epoxy resin as well as hyperbranched polyester (HBP)/RTM6 nanocomposite under compressive loading. Numerical simulations were performed in LS-DYNA by means of a statistical approach that exploits different failure strains among elements. It allows a phenomenological description of the effect of defects and different stress triaxialities on the failure modes of polymer/nanocomposite materials. Additionally, a parameter describing defects, named defect severity, was added to the model in order to quantify and explore the effect of defects on the mechanical behaviours during the damage process. Both the generalized incremental stress-state dependent damage model (GISSMO) and Monte Carlo methods were employed to simulate the effect of stress triaxiality and the spatial distribution of defects on the mechanical performances. The relationship between the defect severity and the failure modes (tensile-domain and shear-domain) was also discussed. Numerical results of neat RTM6 showed that the presence of a large number of defects can lead to more brittle (tensile-domain) failure, while numerical results of HBP/RTM6 nanocomposite showed that the addition of nanoparticles can compensate the negative effect of the existing defects in polymer materials under uniaxial compression, which provides a novel insight for potential applications of nanomaterials.

Keywords: fracture; voids and inclusions; polymeric material; finite element method; stochastic

[i] Preprint created in August, 2021.
The final version can be found on the journal website.

1. Introduction

Despite the fact that polymer materials have been used in our daily life for a long time, further understanding of the mechanical properties of their mechanical behaviour is still required. Recent works presented the potential applications of adding nanoparticles into polymer materials, such as multifunctional applications with respects to electrical (Esmaeili et al., 2020b) and thermal (Zotti et al., 2020) properties, as well as their improved mechanical properties (Esmaeili et al., 2020b, 2020a; Ma et al., 2021b; Zotti et al., 2019, 2020). In order to investigate the effect of adding nanoparticles and to replicate the mechanical/multifunctional response of nanocomposites, attention has been paid to the analysis of the mechanical behaviour and damage process of polymer materials (Ma et al., 2020b) as well as the development of related numerical methods (Esmaeili et al., 2020a; Genckal and Seidel, 2020; Ma et al., 2020c; Wu et al., 2020). However, compared with tensile cases, the compressive case of both polymer materials and polymer-based nanocomposites is less studied due to the complex stress states of the materials while loading (Chevalier et al., 2019b). Therefore, it is of great interest to uncover the multi-state stresses of both polymer materials and polymer-based nanocomposites under compression with the development of a numerical framework.

The compressive behaviours of polymer materials are quite complex according to the existing experimental activities (Chevalier et al., 2016, 2019b; Meijer and Govaert, 2005; Morelle et al., 2017), especially with respect to the failure morphologies. One of the key reasons is the complexity of the stress states with a mixture of tensile, shear and compressive states, that can be simultaneously presented on the sample during uniaxial compression (Narayan and Anand, 2021). Therefore, compared with other simple loading cases, the compressive behaviours of polymer materials are more like structural responses rather than material characterizations, posing challenges on numerical simulations. Generally, the stress-strain curve from the uniaxial compressive tests of polymer materials can be divided into four zones (Chevalier et al., 2019a; Zotti et al., 2020), as shown in Figure 1. The linear relationship between the stress and strain is located in Zone I, indicating the elastic mechanical behaviour of the material. Then, the modulus degrades in Zone II, attributed to the plasticity. After reaching the strength, the material starts to soften and the stress decreases due to the damage of the material corresponding to Zone III. Finally in Zone IV, the stress increases again because a new structure with higher-density fragments forms after the collapse of the polymer materials (Meijer and Govaert, 2005). Such complex compressive behaviours have been reported for RTM6 epoxy resin (Chevalier et al., 2016; Morelle et al., 2017). The research objective of the present work is focused on Zone I to Zone III, while Zone IV was not considered here due to the collapsed structure of polymer materials.

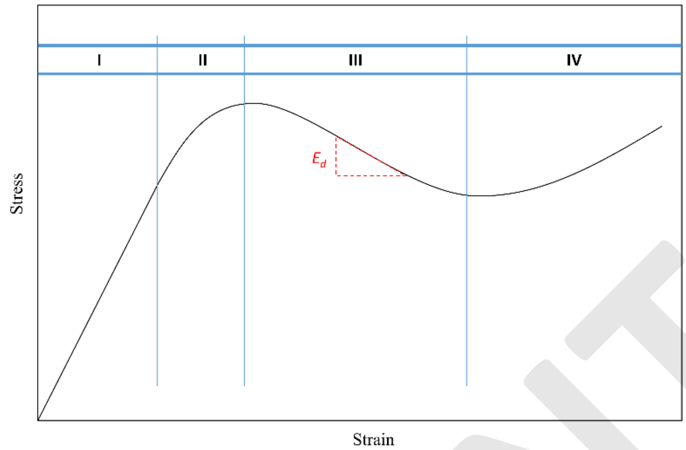

Figure 1 Typical stress-strain curve from the compressive tests of RTM6

An interesting phenomenon was reported by Morelle et al (Morelle et al., 2017) in which two main failure modes of RTM6 epoxy resin were presented, which shared similar four-zone constitutional curves of uniaxial compressive tests. One of failure modes formed crack surfaces along planes oriented at 45° of the loading direction. This failure mode was governed by shear stresses and can be regarded as a typical compressive failure mode of ductile materials; while the other failure mode was similar to the compressive failure mode of brittle materials, in which many cracks were found at the exterior surface of the sample along the initial loading direction and propagated radially and circularly, also known as peeling in some works (Chevalier et al., 2016). Besides the morphology of cracks, the material failed as the first mode experienced stable crack propagations which led to few fragments after the tests, while the material with the second failure mode showed sudden crack propagations and fragmented into many small pieces at the state of the final collapse.

However, the reason why these two different types of failure modes occur simultaneously in the same material system and their relationship are still unclear (Morelle et al., 2017); one explanation could be the existence of defects inside the polymer materials (Ma et al., 2020a; Zhou et al., 2005). Known as (highly) cross-linked materials, polymer materials have complex molecular structures due to their long-chain molecules (Chang et al., 2015; Park and Cho, 2020; Shin et al., 2019), as a result of competing processes from different chemical reactions (Weidner et al., 2019). Due to these reactions, molecular structures are rarely identical, leading to imperfect chains at the molecular level (Zhang and Ray, 1997).

Additionally, defects at the macroscale level, such as impurities (Morcom et al., 2010), voids (Vidler et al., 2021) and scratches (Kurkcu et al., 2012), cannot be avoided during the manufacture process. Because of their significant effects on the mechanical properties, especially on deformation and fracture, both the molecular and macroscale levels of defects should not be neglected during the analysis of polymer materials (Kurkcu et al., 2012; Li et al., 2020; Ma et al., 2020a; Vidler et al., 2021). Through the fractographic analyses of tested RTM6 samples, Chevalier et al. (Chevalier et al., 2019b, 2018) identified the correlation between fracture surfaces and ambient defects. Considering the stochastic distribution of these defects inside polymer materials, homogeneous approaches, like finite element (FE) method, might be unsuitable to accurately describe the uncertainties of mechanical responses (Park and Cho, 2020). However, by applying the Monte Carlo method combined with the introduction of defect-related parameters and statistical distributions (Ma et al., 2021a; Ozturk et al., 2021; Wang et al., 2021), the mechanical response of the polymer materials can be reconstructed in a numerical environment. However, most of the existing works of defect-related analysis focused on the tensile and fracture cases, while compressive cases have been considered less due to the complexity of the fracture behaviours and the failure criteria implemented in the numerical calculation. Therefore, it is meaningful to comprehensively investigate the mechanical response of polymer materials under uniaxial compression with the development of numerical methods, especially with a focus on their fracture performances while also considering defects. Furthermore, better understanding of the mechanism of adding nanoparticles and replicating the mechanical response of nanocomposites under compression is also required.

In the current work, a numerical framework based on the finite element method and Monte Carlo simulations was built to mimic the compressive mechanical behaviours considering the distributions of defects and the damage accumulation process of the RTM6 epoxy with a special focus on Zone III. Following the validation, the numerical model was also employed to investigate the effect of nanoparticles in the polymer materials considering the presence of defects, as analysed in our previous work (Ma et al., 2020a). We used hyperbranched polyester (HBP) as reinforced nanoparticles for the present study, which has a perfect interface with polymer materials (Boogh et al., 1999) to avoid the consideration of bonding strengths (Jensen et al., 2018). Considering that the weight fraction of HBP in the current work was quite low (0.1 wt.%), the effect of the agglomeration of particles and of the defects introduced by nanoparticles are reduced, which significantly increase in case of a higher weight fraction (Esmaeili et al., 2020a). A numerical investigation, aiming to describe the mechanical responses of polymer materials under uniaxial compression with the consideration of defects and nanoparticles, was carried out based on our previous experimental research on HBP/RTM6 (Zotti et al., 2020) analysing fracture behaviours in uniaxial compressive tests of RTM6 (Morelle et al., 2017).

2. Numerical modelling

2.1 Modelling process

In the current numerical framework, in order to better describe the mechanical responses under compressive loading, a FE model, which contains the stress-state-dependent damage model governed by stress triaxiality, was built. Furthermore, Monte Carlo simulation was employed to investigate the existence of the defects and their distributions on the mechanical properties and damage process of polymer materials. The current numerical model was applied on both neat epoxy resin and nanocomposites, i.e. RTM6 and HBP/RTM6, and the simulated results were validated. Additionally, the relationship between the different failure modes and the presence of defects was studied on neat epoxy. And the effect of adding nanoparticles on compressive mechanical behaviours of nanocomposites, by taking into account the variation of the defects inside materials, was explored.

2.2 FE model

A numerical model was built to replicate the experimental setup according to (Morelle et al., 2017; Zotti et al., 2020), as presented in Figure 2. The geometry dimension of the sample in the model corresponds to the experimental specimen with a diameter of 8 mm and a height of 4 mm shaped as a cylinder. Considering the platens, Platen 1 on the top was the loading side to mimic the loading process under a constant velocity as in experiments, while Platen 2 was the supporter of the sample. Constant stress solid element (solid element type 1) was used to model the sample, while the platens were meshed by Belytschko-Tsay shell (shell element type 2) to reduce the calculation time.

Automatic_surface_to surface contact was used to model the contact behaviours between platen 1/2 and the sample, where the contact force was regarded as the loads imposed to the sample. A small friction was assigned between the sample surface and the platens to simulate the friction in the experimental activities and the coefficient was set equal to 0.07 according to the compressive study from Chevalier et al. (Chevalier et al., 2016). The whole modelling process was conducted through LS-DYNA for the present study.

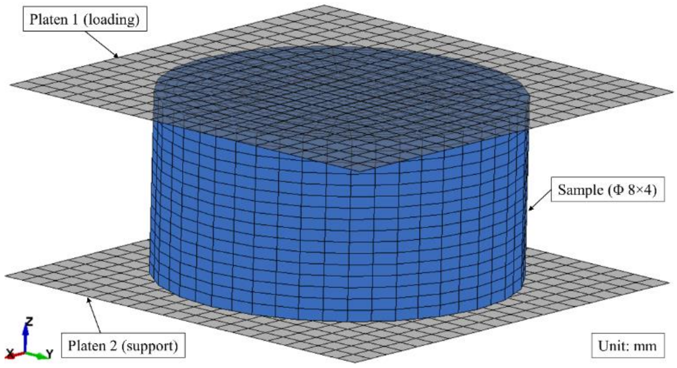

Figure 2 Finite element model for the uniaxial compressive tests

2.3 Material properties

In Zone I, the linear elastic behaviour can be described by the basic mechanical parameters, including the density, Poisson ratio and elastic modulus, as listed in Table 1. Regarding Zone II, the Johnson-Cook model (a simplified one, MAT_098, without damage and failure criteria), was used to mimic the deformation of the sample in Zone II. The related parameters in the material model were fitted based on the experimental data (Zotti et al., 2020) as plotted in Figure 3, and are listed in Table 1. With regards to the platens, a rigid body (MAT_020) was used since there was no deformation on the platens during the whole loading process. All freedoms of Platen 2 were fixed, and they were similar for Platen 1 except that the translation along z-axial which was free.

Table 1 Parameters used to describe the mechanical response of the sample in Zone I & II

	Variable	Parameter	Value
Zone I	Density	ρ (g/cm^3)	1.14
	Elastic modulus	E (MPa)	3000
	Poisson ratio	μ	0.3
Zone II	Parameters for Johnson-Cook model	A	86.23
		B	144.60
		n	0.31

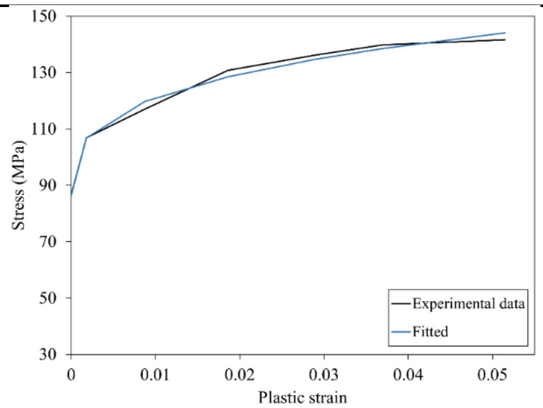

Figure 3 Comparison between the fitted and experimental data in Zone II

2.4 Failure model

Besides the material models, the failure criterion was independently implemented in the simulation to mimic the mechanical behaviours in Zone III. As discussed in the introduction, complex stress states might influence the mechanical property of polymer materials during uniaxial compressive loading. Therefore, a failure criterion considering the triaxiality can describe different failure processes as the stress state differs better. In LS-DYNA, a generalized incremental stress-state dependent damage model (GISSMO) can be employed to identify the failure behaviour of materials considering different stress triaxialities (Manual and Ii, 2012). Particularly, a curve of the plastic failure strain with respects to different stress triaxialities can be assigned to each element; during the calculation, the stress state represented as the stress triaxiality can be checked at each step, and those elements whose strains reach the failure threshold at the current stress state are deleted immediately.

The failure strain with respects to various stress triaxialities for RTM6 epoxy resin is presented in Figure 4. For uniaxial compressive tests, the local stress triaxiality ranges generally between -1/3 and 1/3 during loaded. Therefore, a varied failure strain with stress triaxialities ranging from -1/3 to 1/3 is used in the present numerical model to control the element deletion. The plastic failure strains at different stress triaxialities, see Figure 4, were extracted from related tests (Morelle et al., 2017). The plastic failure strain from pure compression was used when a stress triaxility equal to -1/3. As for the stress state of torsion with a stress triaxiality between -1/3 and 0, the plastic failure strain was obtained from the maximum value of the existing experimental data from torsion tests (Morelle et al., 2017). In addition, for all these failure strains, the maximum value in each stress state was employed instead of the mean value of all the available experimental data. This choice was made in order to introduce defects to the current work.

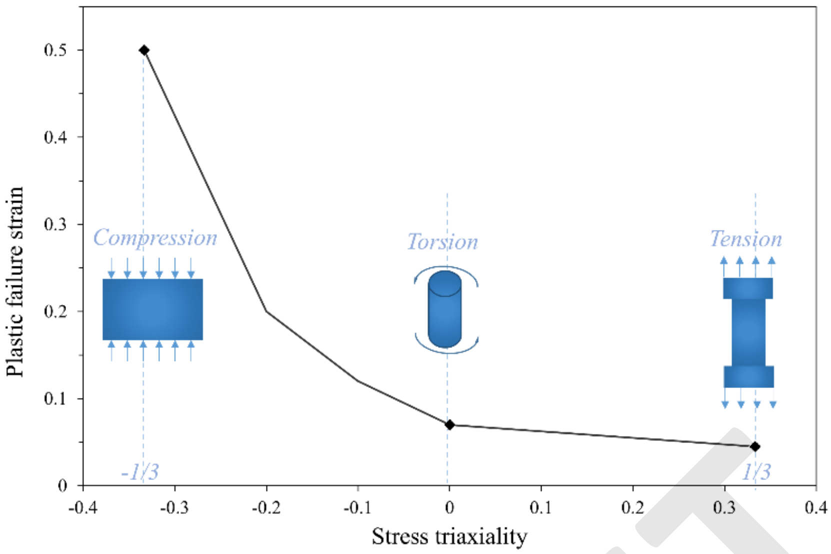

Figure 4 Plastic failure strain with respects to the stress triaxiality

2.5 Consideration of defects

According to existing numerical models which consider defects of polymer materials (Ma et al., 2020a; Zhou et al., 2005), an earlier failure process was presented due to the presence of the relationship between the crack initiation and ambient defects as reported in (Chevalier et al., 2019b). Thus, the failure strain with respects to stress triaxiality may be lower because of defects. Elements with a different number of defects can have a different stress-state-dependent failure strain (see the curves representing different number of defects in Figure 5a). Elements with more defects have a lower failure strain for the same stress triaxiality. In order to quantitatively investigate the effect of defects on the mechanical and failure behaviours of RTM6 epoxy resin, an evaluation of the defect severity was built as shown in Figure 5b. Here, the defect severity, Ω, presented in percentage, quantifies how significantly the presence of defects affects the failure strain at a local region of the material. If the sample contains local defects with a maximum defect severity, Ω_{max}, a normal distribution of the failure strain ratio, R_f, between 1 (the failure strain without the defects), and (100% - Ω_{max}) can be constructed. So given a certain Ω_{max}, a normal distribution with a failure strain ratio ranging from 1 to (100% - Ω_{max}) can be assigned to the model, based on which related parameters vary from element to element. Herein, the failure strain ratio R_f, which is the ratio of the failure strain with the defects to the failure strain without defects is also introduced in Figure 5b, correlated to Ω_{max}. Herein, it is assumed that elements with the defect severity Ω present the R_f equal to (100% - Ω). So, a higher Ω will relate to lower R_f and a lower failure strain compared with the non-defect case.

Taking into account the Ω - R_f relationship mentioned above, for a known Ω_{max} the distribution of Ω can be converted into the distribution of R_f. This conversion is based on stress triaxiality-failure strain curve assigned to the element in the current numerical model through stochastic settings, named as Define_Stochastic_Variation in LS-DYNA. A specific example of assigning the distribution and creating the relationships is presented in Figure 5c. Thus, coupled with GISSMO, a stochastic stress-state-dependent failure strain can be assigned to each element following a specific statistical distribution, as visible in Figure 5c. For the same statistical distribution of the defect severity, a non-deterministic random number generator ("LS-DYNA Keyword User's Manual," 2018) was used to mimic the spatial randomness of Ω among elements with the assistance of the Monte Carlo method as the examples presented in Figure 5d. An overall flowchart with the main features of the current numerical framework is presented in Figure 5. However, as noticed, the introduction of defects to the model highlights the importance of the mesh sensitivity. By studying the mesh size for models with a defect severity of Ω_{max} = 0, 60% and 70%, which were mainly used in the current work, the mesh size in the present models was set to 0.5 mm considering the balanced accuracy and efficiency.

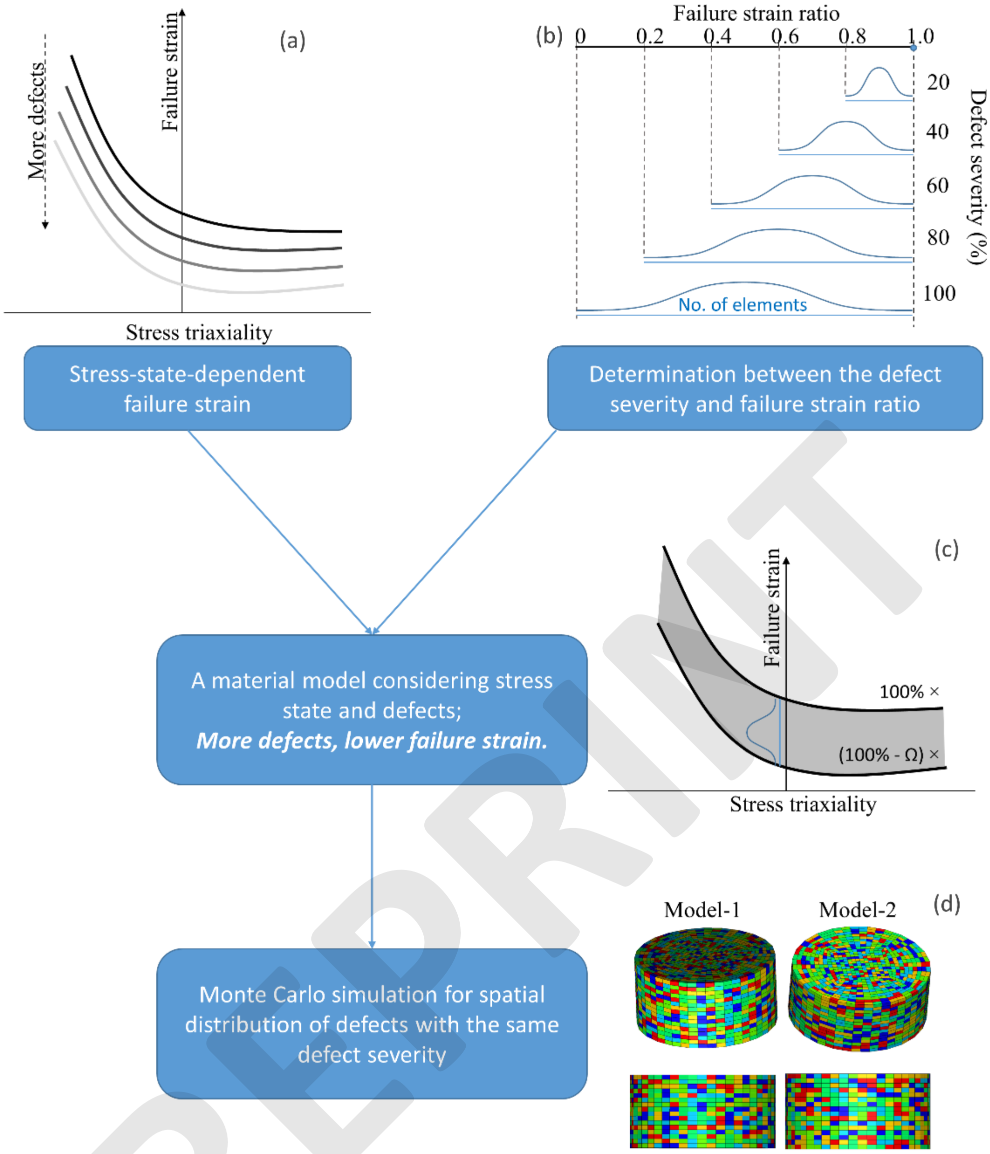

Figure 5 Main features of the current modelling strategy: different failure strains with respects to the stress triaxiality considering defects (a); the relationship between the distribution of the failure strain and the defect severity (b); an example of the assignment of the failure strain with respects to the distribution of defects (c); models for different spatial distribution of defects with the same severity (d)

Regarding modelling HBP/RTM6 nanocomposites, cracks tend to close under compression according to typical fracture mechanisms (Broek, 2012), and this closure weakens the reinforcement provided by nanoparticles (Esmaeili et al., 2020b). Thus, the effect of nanocomposites on defect severity should be stressed for compressive simulations. Therefore, in order to establish the relationship between the defect severity and the addition of nanoparticles, we varied the defect severity to mimic the mechanical behaviours of nanocomposites under compression until a specific defect severity with good agreement with the experimental data of nanocomposites was obtained. Through this method, the effect of nanoparticles on the mechanical properties of polymer materials can be described by the defect severity in the current numerical framework. More details of nanocomposites can be found in the following section.

3. Results and discussion

3.1 Effect of defects on constitutional curves

Through changing the maximum defect severity from 0% to 90% in the numerical models, different stress-strain curves were obtained as plotted in Figure 6a. In each case of defect severity, 100-time Monte Carlo simulations were performed to consider the stochastic spatial distribution of the defects inside the polymer. The stress-strain relation in Zone I and II is almost identical with varying defect severities while obvious differences are visible in Zone III. As Zone III is dominated by the damage accumulation process, it is more sensitive to the defect severity inside the polymers compared with Zone I and II, determined by the elastic-plastic material models based on our experimental results (Zotti et al., 2020). Thus, the current analysis and discussions were focused on Zone III, the damage-related region of the constitutional curve.

For the model without defect (see 0% in Figure 6a), a minimal damage can be found near the platens, accompanied by the typical plastic behaviour without any stress reduction as the strain increases. Regarding models with defects, the stress reduction becomes more pronounced as the defect severity increases, in line with the fact that the presence of more defects leads to quicker failure of the sample. The damage slope, E_d, which is the slope of the stress-strain curves in Zone III ($E_d > 0$, when defect severity is 0; $E_d < 0$, when defects severity is greater than 0), is summarized in Figure 6b with regards to different defect severity considering the variation from Monte Carlo simulations. The change of the damage slope was significant when the defect severity was close to 0 and 90%, while the trend was smooth within a medium percentage. As a limited defect severity was introduced to the model (value close to 0), obvious differences were produced on the stress: the strain varied from 0.1 to 0.2 as the damage process is accelerated with a lower failure initiation strain provided by defects. With considerable defects inside the model (value close to 90%), the crack density/failed elements could rapidly reach saturation followed by the collapse of the sample, indicating a significant decrease of the damage slope in Figure 6b near 100%. For a defect severity between 10% and 70%, the damage process is stable which shows a slowly dropping trend of E_d in Figure 6b. Additionally, there is also a small visible variation of the damage slope, which barely affects the overall trend of E_d, as presented by the error bar in Figure 6b, due to the spatial distribution of defects considered by Monte Carlo simulations in the current work.

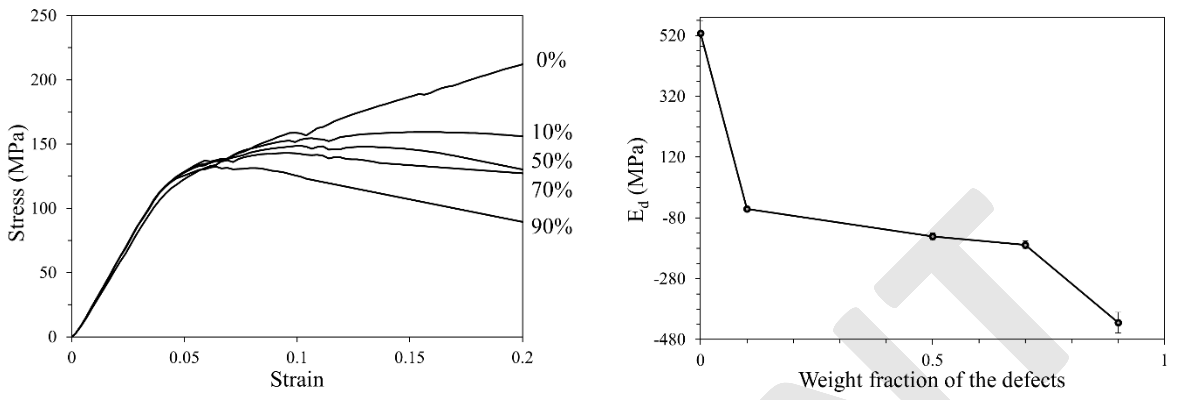

(a) *(b)*

Figure 6 Stress-strain curves with different defect severity (a); relationship between the slope in the damage zone of the stress-strain curve and the defect severity (b)

3.2 Effect of defects on failure modes

For the neat RTM6 epoxy resin, the stress-strain curve from the numerical model with 70% defects matches the curve from the experimental activities well (Zotti et al., 2020) with a special focus on Zone III, as shown in Figure 7a. Considering the good agreement between numerical and test data, tested samples employed in experimental activities corresponded to the numerical model with 70% defects. The damage slope, E_d, from 100-time Monte Carlo simulation is presented in Figure 7b, showing that the experimental damage slope is quite close to the average value from the numerical model with a variation of ± 8%, also as visible in Figure 6b.

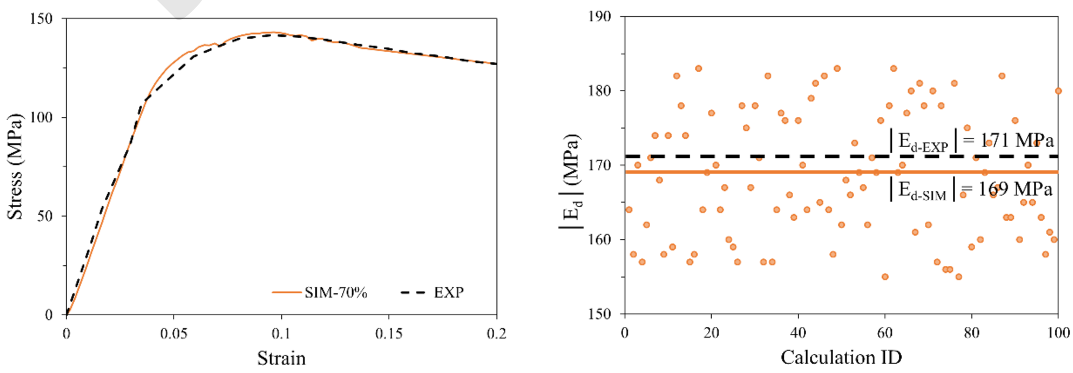

(a) *(b)*

Figure 7 A good agreement between the numerical results with 70% defect severity and experimental data (a); comparison experimental damage modulus with numerical ones including Monte Carlo calculations and average value (b)

After validating the numerical model with 70% defects by the experimental stress-strain curve, the failure modes are discussed here. As aforementioned in the introduction, two different failure modes under uniaxial compression were reported from existing experimental works, presented as crack surfaces along planes oriented 45° of the loading direction and straight cracks along the loading direction propagating radially and circularly, named as Mode-A and Mode-B. Given the same defect severity 70% in the modelling of nanocomposite, these failure morphologies were also obtained during Monte Carlo simulations, as seen in Figure 8. At the final failure stage, the sample collapses into several parts with a 45° crack for Mode-A, while lots of fragments are formed in the numerical results of Mode-B failure morphology with straight cracks presented along the loading direction. In order to clearly present the crack morphologies, we removed the deformation in the post analysis of the numerical results, which are shown in Figure 8. According to the experimental activities reported by Morelle et. al. (Morelle et al., 2017), crack morphologies provided by simulations are in a good agreement with the experimental data (with a white dashed line to mark the crack in the image captured from tests (Morelle et al., 2017)).

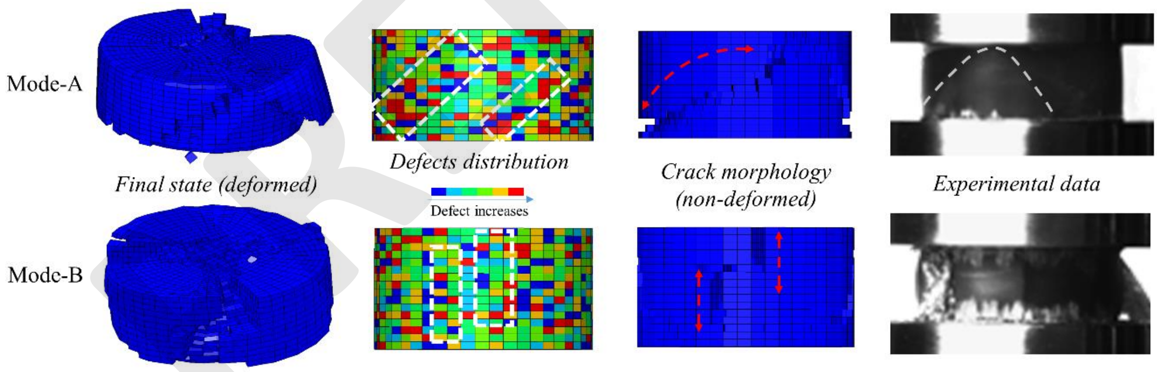

Figure 8 Two failure morphologies from numerical results compared with the experimental ones (Morelle et al., 2017)

The formation of both failure modes is related to the spatial distribution of the defects (see Figure 8) in the model for the same severity, which determines the stress triaxiality among the elements at the first step of the numerical-explicit analysis. The increase of the analysing steps leads to a continuous change of the stress triaxiality of each element due to the increase of the compressive load and local failure (element deletion). So theoretically, both defect severity and stress triaxiality determine the failure strain of an element and later the failure modes of the model. However, the region with a similar defect severity for both Mode-A and Mode-B (see white rectangle in Figure 8) indicated the most probable direction of crack propagation.

As reported in related experimental activities (Morelle et al., 2017), failure of pure Mode-A was observed in samples, while pure Mode-B was rarely present and Mode-B always coexisted with Mode-A in one sample during the loading. The same phenomena occurred also in our numerical results. Based on the numerical results with Mode-B, straight cracks initiated earlier than cracks with a 45°orientation. Straight cracks undergo tension-domain failure and exhibit a lower failure strain than 45° cracks that that undergo shear-domain failure. With regards to the propagation of cracks, straight cracks were quite unstable and easily affected by the defects on the propagated paths, leading to the branching of cracks and resulting in the presence of a mixture of straight and 45° cracks. Therefore, samples with the involvement of Mode-B failure can produce more fragments with smaller sizes compared with samples in pure Mode-A failure, which is in line with conclusions drawn in (Morelle et al., 2017).

These two different failure modes with the proportion of both modes in all Monte Carlo simulations were quantified in Figure 9 with different defect severity. Due to the fact that Mode-B failure always occurs in combination with Mode-A, Mode_B is defined with straight cracks as their main failure mode. All the data used for the collection of proportions was obtained through 100-time calculations. As the defect severity increases, a linear increase of Mode-B failure cases can be found in the simulated results. Herein, we can regard the Mode-B, with straight cracks with tension-domain failure, as the brittle failure (Morelle et al., 2017). As known, samples with more defects tend to fail as brittle materials (Ma et al., 2020a).

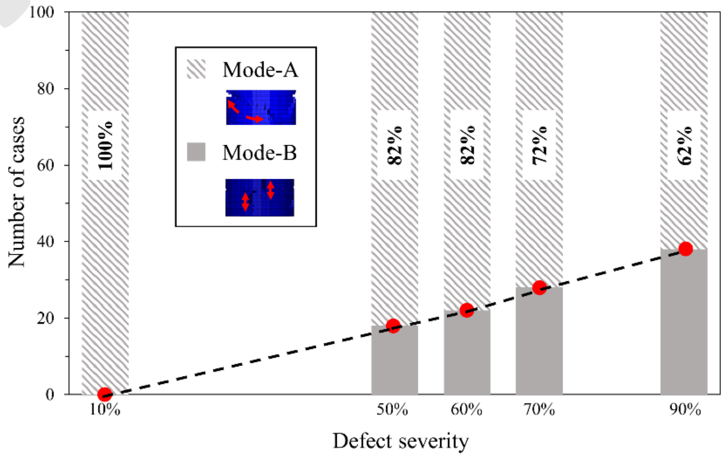

Figure 9 Proportion of two crack modes with respects to different defect severity

3.3 Effect of nanoparticles on compressive behaviours

Here, RTM6 reinforced with 0.1 wt.% HBP nanoparticles under compression is further analysed based on the modelling of neat RTM6 with different defect severities. The basic idea was to model the mechanical properties of HBP/RTM6 nanocomposite by tuning the defect severity. A proper defect severity can then be found through comparing the modelled mechanical properties with the experimental data, which could help to establish a relationship between the addition of nanoparticles and the defect severity. As observed in Figure 10, the experimental stress-strain curve is in good agreement with the numerical results when ~60% of the defect severity is used in the modelling. In fact, the difference between the models, with and without the HBP, on the stress-strain curves of Zone I and II is not obvious based on the results from (Zotti et al., 2020), but is mainly located in the damage process (Zone III). Therefore, the good agreement presented in Figure 10a, especially in Zone III, indicates that the mechanical behaviour of the nanocomposites with 0.1 wt.% HBP fits with the sample with less defects (~60%) well compared with the neat RTM6 (70% defects). Therefore, the addition of nanoparticles can somehow compensate the negative effect of defects on the compressive responses. As visible in Figure 10b, the mechanisms of reinforcement provided by nanoparticles are different under loading conditions with different stress triaxialities. Under tensile loading, the good bonding between the matrix and nanoparticles can induce a reinforcing mechanism known as bridging (Esmaeili et al., 2020a), which can prevent crack propagation and can lead to a high fracture toughness. As for the shear conditions, nanoparticles reinforce the fracture properties but not significantly (Li et al., 2019). However, considering nanocomposites under compression, the effect of nanoparticle is less obvious because cracks close during loading after the initiation (Broek, 2012). Therefore, the difference of the stress-strain curves with and without nanoparticles for the compression tests should be insignificant for Zone I and II, but the introduction of nanoparticles can somehow reduce the effect of existing defects on the mechanical properties of the polymer materials according to the current numerical investigations, which then leads to a decrease of the defect severity for 0.1 wt.% nanocomposite from 70% to 60% compared with the neat one. Even though the reinforcement of the compressive modulus and strength by nanoparticles on RTM6 is insignificant, the mechanism by which nanoparticles compensate the negative effect of defects and affect the damage process provides new insights into the potential application of nanomaterials.

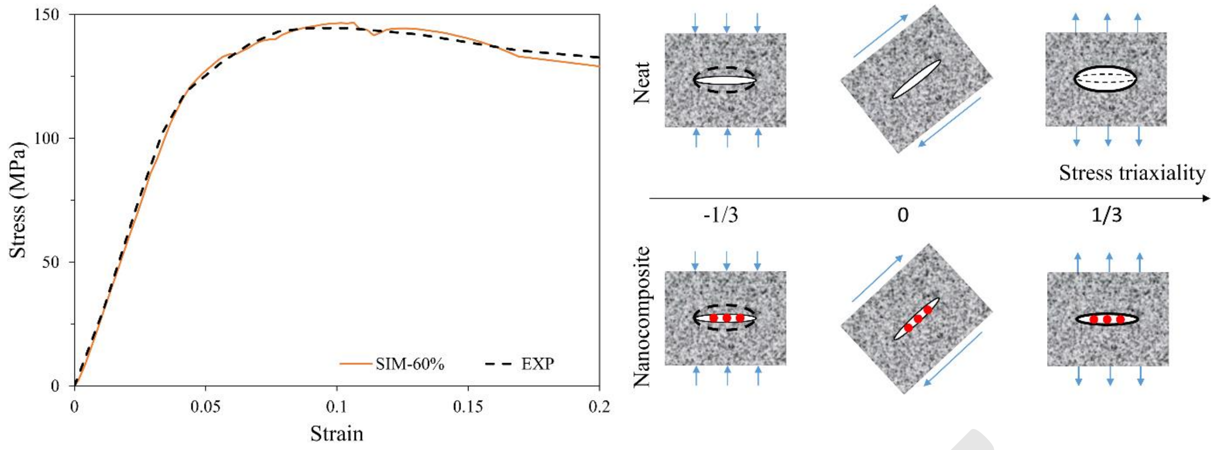

(a) *(b)*

Figure 10 Comparison of the stress-strain curves from experiments with 0.1 wt.% and numerical model with 60% defects (a); Schematic about the mechanism with nanoparticles (b)

4. Conclusion

A modelling strategy was proposed containing a FE method and Monte Carlo simulations to study the relationship between defects and the damage process of RTM6 and HBP/RTM6 nanocomposites under uniaxial compression. In order to consider the presence of defects inside polymer materials and the complex stress states in uniaxial compressive loading of polymer materials, a stochastic numerical framework with defect severity and stress-state-dependent failure criterion was built. Monte Carlo simulations were conducted to investigate the effect of the spatial distribution of defects on the damage process. Regarding polymer materials with nanoparticles, a different defect severity was used to describe the mechanical behaviours of nanoparticle-reinforced polymers as the bridging mechanisms from nanoparticles is not significant due to the closure of cracks in materials under compression. The numerical methodology can, however, be used to investigate the effect of defects on the mechanical behaviours.

In the present work, based on the stress-strain curves and failure modes from related experimental activities, the discussion of the effect of defects on the mechanical properties of polymer materials (RTM6) and the introduction of nanoparticles (HBP) on the mechanical behaviours and failure modes under uniaxial compression has been explored through the proposed modelling strategy. The main conclusions that can be drawn are the following:

- The current numerical framework considering the defect severity and stress state has been validated for polymer materials under uniaxial compressive loading.

- The existing defects in polymer materials mainly affect the damage part (Zone III) of the stress-strain curves under compressive loading.
- Two different failure modes with shear-domain and tension-domain cracks are observed during 100-times Monte Carlo simulations due to the spatial distribution of defects, in line with experimental findings.
- The introduction of defect severity in the current numerical work shows that the addition of nanoparticles into the polymer material can somehow compensate the negative effect of existing defects on compressive mechanical responses.

Furthermore, specific for nanoparticle-reinforced polymer materials, even though the compensation of defects through the addition of nanoparticles difficult to validate in experimental works considering the defects from different scales, the current work on nanoparticles provides a new insight for the investigation of nanocomposites, especially under compression, of which the effect of nanoparticles is believed to be insignificant.

References

Boogh, L., Pettersson, B., Månson, J.A.E., 1999. Dendritic hyperbranched polymers as tougheners for epoxy resins. Polymer (Guildf). 40, 2249–2261. https://doi.org/10.1016/S0032-3861(98)00464-9

Broek, D., 2012. The practical use of fracture mechanics. Springer Science & Business Media.

Chang, B., Wang, B., Zheng, G., Dai, K., Liu, C., Shen, C., 2015. Tailoring microstructure and mechanical properties of injection molded isotactic-polypropylene via high temperature preshear. Polym. Eng. Sci. 55, 2714–2721. https://doi.org/10.1002/pen.24078

Chevalier, J., Brassart, L., Lani, F., Bailly, C., Pardoen, T., Morelle, X.P., 2018. Unveiling the nanoscale heterogeneity controlled deformation of thermosets. J. Mech. Phys. Solids 121, 432–446. https://doi.org/10.1016/j.jmps.2018.08.014

Chevalier, J., Camanho, P.P., Lani, F., Pardoen, T., 2019a. Multi-scale characterization and modelling of the transverse compression response of unidirectional carbon fiber reinforced epoxy. Compos. Struct. 209, 160–176. https://doi.org/10.1016/J.COMPSTRUCT.2018.10.076

Chevalier, J., Morelle, X.P., Bailly, C., Camanho, P.P., Pardoen, T., Lani, F., 2016. Micro-mechanics based pressure dependent failure model for highly cross-linked epoxy resins. Eng. Fract. Mech. 158, 1–12. https://doi.org/10.1016/J.ENGFRACMECH.2016.02.039

Chevalier, J., Morelle, X.P., Camanho, P.P., Lani, F., Pardoen, T., 2019b. On a unique fracture micromechanism for highly cross-linked epoxy resins. J. Mech. Phys. Solids 122, 502–519. https://doi.org/10.1016/j.jmps.2018.09.028

Esmaeili, A., Ma, D., Manes, A., Oggioni, T., Jiménez-Suárez, A., Ureña, A., Hamouda, A.M.S., Sbarufatti, C., 2020a. An experimental and numerical investigation of highly strong and tough epoxy based nanocomposite by addition of MWCNTs: Tensile and mode I fracture tests. Compos. Struct. 252, 112692. https://doi.org/10.1016/j.compstruct.2020.112692

Esmaeili, A., Sbarufatti, C., Ma, D., Manes, A., Jiménez-Suárez, A., Ureña, A., Dellasega, D., Hamouda, A.M.S., 2020b. Strain and crack growth sensing capability of SWCNT reinforced epoxy in tensile and mode I fracture tests. Compos. Sci. Technol. 186, 107918. https://doi.org/10.1016/j.compscitech.2019.107918

Genckal, N., Seidel, G.D., 2020. Multiscale Modeling of Damage Response in Nanocomposites Reinforced with Carbon Nanotubes. AIAA Scitech 2020 Forum 1–12. https://doi.org/10.2514/6.2020-1380

Jensen, B.D., Odegard, G.M., Kim, J.-W., Sauti, G., Siochi, E.J., Wise, K.E., 2018. Simulating the effects of carbon nanotube continuity and interfacial bonding on composite strength and stiffness. Compos. Sci. Technol. 166, 10–19. https://doi.org/10.1016/J.COMPSCITECH.2018.02.008

Kurkcu, P., Andena, L., Pavan, A., 2012. An experimental investigation of the scratch behaviour of polymers: 1. Influence of rate-dependent bulk mechanical properties. Wear 290–291, 86–93. https://doi.org/10.1016/j.wear.2012.05.005

Li, X., Saeedifar, M., Benedictus, R., Zarouchas, D., 2020. Damage Accumulation Analysis of CFRP Cross-Ply Laminates under Different Tensile Loading Rates. Compos. Part C Open Access 100005. https://doi.org/10.1016/j.jcomc.2020.100005

Li, Y., Wang, Q., Wang, S., 2019. A review on enhancement of mechanical and tribological properties of polymer composites reinforced by carbon nanotubes and graphene sheet: Molecular dynamics simulations. Compos. Part B Eng. 160, 348–361. https://doi.org/10.1016/J.COMPOSITESB.2018.12.026

LS-DYNA Keyword User’s Manual, 2018.

Ma, D., Campos Amico, S., Giglio, M., Manes, A., 2021a. Effect of fibre bundle uncertainty on the tensile and shear behaviour of plain-woven composites. Compos. Struct. 259, 113440. https://doi.org/10.1016/j.compstruct.2020.113440

Ma, D., Elmahdy, A., Verleysen, P., Giglio, M., Manes, A., 2020a. A cohesive-based method to bridge the strain rate effect and defects of RTM-6 epoxy resin under tensile loading. Procedia Struct. Integr. 28, 1193–1203. https://doi.org/10.1016/j.prostr.2020.11.101

Ma, D., Esmaeili, A., Manes, A., Sbarufatti, C., Jiménez-Suárez, A., Giglio, M., Hamouda, A.M., 2020b. Numerical study of static and dynamic fracture behaviours of neat epoxy resin. Mech. Mater. 140, 103214. https://doi.org/10.1016/J.MECHMAT.2019.103214

Ma, D., Giglio, M., Manes, A., 2020c. An investigation into mechanical properties of the nanocomposite with aligned CNT by means of electrical conductivity. Compos. Sci. Technol. 188, 107993. https://doi.org/10.1016/J.COMPSCITECH.2020.107993

Ma, D., González-Jiménez, Á., Giglio, M., dos Santos Cougo, C.M., Amico, S.C., Manes, A., 2021b. Multiscale modelling approach for simulating low velocity impact tests of aramid-epoxy composite with nanofillers. Eur. J. Mech. - A/Solids 104286. https://doi.org/10.1016/j.euromechsol.2021.104286

Manual, K.U.S., Ii, V., 2012. Keyword User ’ S Manual Volume Ii.

Meijer, H.E.H., Govaert, L.E., 2005. Mechanical performance of polymer systems: The relation between structure and properties, in: Progress in Polymer Science (Oxford). Pergamon, pp. 915–938. https://doi.org/10.1016/j.progpolymsci.2005.06.009

Morcom, M., Atkinson, K., Simon, G.P., 2010. The effect of carbon nanotube properties on the degree of dispersion and reinforcement of high density polyethylene. Polymer (Guildf). 51, 3540–3550. https://doi.org/10.1016/J.POLYMER.2010.04.053

Morelle, X.P., Chevalier, J., Bailly, C., Pardoen, T., Lani, F., 2017. Mechanical characterization and modeling of the deformation and failure of the highly crosslinked RTM6 epoxy resin. Mech. Time-Dependent Mater. 21, 419–454. https://doi.org/10.1007/s11043-016-9336-6

Narayan, S., Anand, L., 2021. Fracture of amorphous polymers: A gradient-damage theory. J. Mech. Phys. Solids 146, 104164. https://doi.org/10.1016/j.jmps.2020.104164

Ozturk, D., Kotha, S., Ghosh, S., 2021. An uncertainty quantification framework for multiscale parametrically homogenized constitutive models (PHCMs) of polycrystalline Ti alloys. J. Mech. Phys. Solids 148, 104294. https://doi.org/10.1016/j.jmps.2021.104294

Park, H., Cho, M., 2020. A multiscale framework for the elasto-plastic constitutive equations of crosslinked epoxy polymers considering the effects of temperature, strain rate, hydrostatic pressure, and crosslinking density. J. Mech. Phys. Solids 142, 103962. https://doi.org/10.1016/j.jmps.2020.103962

Shin, H., Choi, J., Cho, M., 2019. An efficient multiscale homogenization modeling approach to describe hyperelastic behavior of polymer nanocomposites. Compos. Sci. Technol. https://doi.org/10.1016/J.COMPSCITECH.2019.03.015

Vidler, J., Kotousov, A., Ng, C.-T., 2021. Effect of randomly distributed voids on effective linear and nonlinear elastic properties of isotropic materials. Int. J. Solids Struct. https://doi.org/10.1016/j.ijsolstr.2021.01.009

Wang, Z., Fu, J., Manes, A., 2021. Discrete fracture and size effect of aluminosilicate glass under flexural loading: Monte Carlo simulations and experimental validation. Theor. Appl. Fract. Mech. 111, 102864. https://doi.org/10.1016/j.tafmec.2020.102864

Weidner, M.C., Evenson, Z., Zamponi, M., Possart, W., 2019. Molecular Motion in Viscous DGEBA with Nanoparticles as Seen by Quasi-Elastic Neutron Scattering. Macromol. Chem. Phys. 220, 1800275. https://doi.org/10.1002/macp.201800275

Wu, P., Zhao, J., Chen, Z., Bobaru, F., 2020. Validation of a stochastically homogenized peridynamic model for quasi-static fracture in concrete. Eng. Fract. Mech. 237, 107293. https://doi.org/10.1016/j.engfracmech.2020.107293

Zhang, S.X., Ray, W.H., 1997. Modeling of imperfect mixing and its effects on polymer properties. AIChE J. 43, 1265–1277. https://doi.org/10.1002/aic.690430515

Zhou, F., Molinari, J.F., Shioya, T., 2005. A rate-dependent cohesive model for simulating dynamic crack propagation in brittle materials. Eng. Fract. Mech. 72, 1383–1410. https://doi.org/10.1016/j.engfracmech.2004.10.011

Zotti, A., Elmahdy, A., Zuppolini, S., Borriello, A., Verleysen, P., Zarrelli, M., 2020. Aromatic Hyperbranched Polyester/RTM6 Epoxy Resin for EXTREME Dynamic Loading Aeronautical Applications. Nanomaterials 10, 188. https://doi.org/10.3390/nano10020188

Zotti, A., Zuppolini, S., Borriello, A., Zarrelli, M., 2019. The effect of glassy and rubbery hyperbranched polymers as modifiers in epoxy aeronautical systems. Compos. Part B Eng. 169, 88–95. https://doi.org/10.1016/j.compositesb.2019.04.006